Mathematical modelling for viscoinelastic nanofluid flow over a stretching sheet with machine learning: an application to tissue adhesive

Article *in* International Journal of Modelling and Simulation · August 2024

DOI: 10.1080/02286203.2024.2392221

3 authors, including:

M. Vanitha Archana
PSG College of Arts and Science
13 PUBLICATIONS **127** CITATIONS
SEE PROFILE

Saeid Jafari
Mathematical and Physical Science Foundation 4200 Slagelse Denmark http://top…
588 PUBLICATIONS **3,345** CITATIONS
SEE PROFILE

Mathematical modelling for viscoinelastic nanofluid flow over a stretching sheet with machine learning: an application to tissue adhesive

P.Priyadharshini[a] , M.Vanitha Archana[b] and Saeid Jafari[c]

[a,b]Department of Mathematics, PSG College of Arts and Science, Coimbatore-641014, Tamil Nadu, India; [c]Mathematical and Physical Science Foundation, 4200 Slagelse, Denmark.

ARTICLE HISTORY
Compiled August 8, 2024

ABSTRACT
The medicated tissue adhesive on a stretching surface through Prandtl-Eyring nanofluid flow is emphasized in the current article to estimate the heat transfer rate and optimize the adhesion process. The effects of Brownian motion and thermophoresis on electrically conducting viscoinelastic nanofluid are taken into consideration with the sight of convective states. The modeled governing equations are nondimensionalized by operating similarity variables to stimulate the optimization process. The result of an executed model is solved scientifically by employing the NDSolve technique. The influence of various parameters on the fluid momentum, thermal, and concentration distributions is accentuated through graphs. Furthermore, the machine learning approach is enhanced to analyze the physical quantities of interest in the entire region. The outcomes are validated to those that have already been published in the pertinent area literature to determine the effectiveness of viscoinelastic nanofluid. The findings revealed that the Prandtl-Eyring fluid parameter enhances the momentum, while the Hartmann number indicates the reverse trend. In addition, it delivers that the proposed machine learning model is capable of forecasting the physical quantities with lower error (10^{-3}) and is a powerful engineering tool that can be effectively employed in a viscoinelastic nanofluid.

KEYWORDS
Machine Learning; Stretching Sheet; Tissue Adhesive; Viscoinelastic Nanofluid
2010 AMS 65G20; 76A05; 76Z99.

1. Introduction

The stretching sheet flow phenomena are of significant value for engineering and medicine owing to the potential applications like polymer sheet extrusion from tubes, metallurgy processes, boundary layer along liquid film concentration process, nuclear reactor safety, drug-delivery systems, and other medical applications. Enlightened by such applications, numerous experimenters are still examining the impact of heat and mass transmission in fluid flow past a stretching sheet. An initial investigation of boundary layer performance on continuous solids with flat surfaces was conducted by Sakiadis [1]. After a few years, it was expanded by Tsou et al. [2], who experimentally analyzed the heat transfer in boundary layer flow and verified the results. Crane [3] has undertaken pioneering research on the exploration of linear and exponential stretching sheets. He developed the idea for steady, incompressible fluid flow in a stated phenomenon and provided an analytical form solution that was exactly equivalent. Zeeshan et al. [4] numerically scrutinized the convective fluid flow with internal heat transfer across a stretchable surface and revealed that the improving Hartmann number reduces the thickness of the boundary layer and surface mass transfer. In another article, Aljaloud et al. [5] conducted a study on the thermal impact of a cross nanofluid over a stretching cylinder and found out that the thermal profile enhanced for a

CONTACT P.Priyadharshini. Email: priyadharshinip@psgcas.ac.in

higher thermophoresis parameter, while decreased for higher values of the Prandtl number. An essential insight into the dynamics of nanofluids over a stretching surface with convection flow ideas are found in recent sources, including [6–18]. These research works offer a greater understanding and explain how the considered flow phenomenon behaves under various conditions.

In the fields of science and engineering, non-Newtonian fluids are more appropriate than viscous fluids for exemplifying the attributes of complex rheological fluids. A premise of Newtonian fluid manners is not always simple, but it may be more complex and necessitate the use of a perturbed (non-Newtonian) model in other cases. The behavior of non-Newtonian is exhibited in various liquid materials like glue, blood, toothpaste, paints, and ketchup. They are classified into two categories: viscoelastic and viscoinelastic. The present research focuses on the assessment of viscoinelastic fluid. The majority of viscoinelastic fluids exhibit similar characteristics at zero shear stress. When exposed to stress, these features react in incredibly unanticipated ways. Researchers have proposed distinct models for an in-depth understanding of the physical factors of considered fluid, involving the power law, Prandtl fluid, and Prandtl-Eyring fluid designs. The Prandtl-Eyring fluid model is a nonlinear flow model that describes the mixed convection state and incorporates activation energy. It was examined by Patil and Goudar [19] over a vertical conical surface. Also, they found that this fluid reduces the surface friction and fluid velocity than the Newtonian fluids. Chaudhary and Chouhan [20] conducted a comprehensive investigation on the Darcy-Forchheimer and electromagnetic-hydrodynamic flow of a Prandtl-Eyring nanofluid over a Riga plate with variable thickness. Puneeth et al. [21] did the study on the bioconvective flow of non-Newtonian fluid through an expanding sheet with the porous medium by considering two major mechanisms, named Brownian motion and thermophoresis. They concluded that the upsurge in the thermophoresis parameter improves the temperature and concentration fields. In addition to the above literature, only a few authors worked Prandtl-Eyring nanofluid model [22–26]. After getting motivated by these references, the Prandtl-Eyring fluid is taken into account for the investigation.

To obtain the solutions of the nanofluid flow models, few authors employed the NDSolve technique, which stands out as a significant numerical approach for addressing ordinary differential equations (ODEs). For instance, Hayat et al. [27] conducted simulation for embedded parameters employing this scheme on the peristaltic flow of Sisko nanofluid in a flexible curved channel and found higher accuracy in the momentum, thermal, concentration, and heat transfer coefficient profiles. Ullah et al. [28] performed and tested the above-mentioned scheme for the nanofluid flow between two parallel plates using a rotating system. Nasir et al. [29] studied the Darcy Forchheimer two-dimensional nanofluid past a stretchable sheet and achieved the solutions by employing HAM and NDSolve. They compared both techniques and found an exceptional similarity. After obtaining knowledge from the previous literatures, this paper emphasized the NDSolve to simulate the two-dimensional Prandtl-Eyring nanofluid flow model. The reason is that the precision and speed of this methodology are well-balanced, and it also necessitates fewer function evaluations with the simplicity of its execution. In addition to that it provides the finest outcomes within the least amount of CPU time. Due to these major advantages, it is selected and coded to provide better accuracy from a few previously issued sources with the help of MATHEMATICA software. Also, the main aim of this work is to test and compare the findings with other computation techniques, namely the Runge-Kutta-based shooting technique, homotopy perturbation method, and implicit finite difference method with the quasi-linearization technique.

In many recent studies, Machine Learning (ML) takes full consideration among researchers and innovators because of its wide range of applications, such as wind energy [30–32], solar energy [33,34], and renewable energy systems [35]. The ML algorithms are divided into three categories: Supervised Machine Learning, Unsupervised Machine Learning, and Semi-supervised Machine Learning, depending on the data type [36,37]. Brenner et al. [38] investigated the role of machine learning in the advancement of fluid mechanics. He fascinated the backstory of the connection between machine learning and fluid mechanics. From a different angle, ML has the potential to be more computationally efficient than physics-based numerical simulations and produce predictions at a fraction of the cost of the original calculation time without compromising accuracy [39–41]. Inspired by the existing literature, the pro-

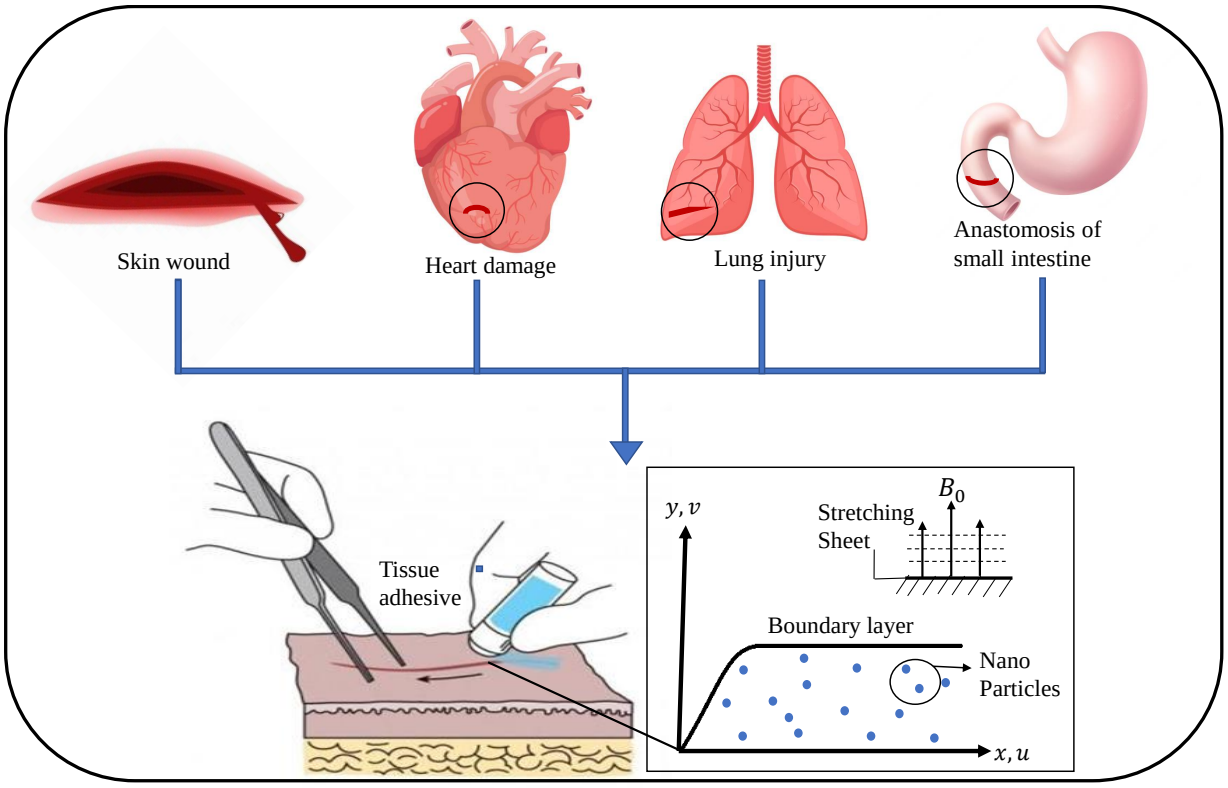

Figure 1. Medicated tissue adhesive on various surgeries with geometry of the problem.

posed work employed the ML algorithm to handle numerous issues in fluid research, including parameter extraction, statistical metrics of error analysis, and overcoming the inherent computation complexity.

Hemorrhage has been identified as the primary cause of death within the first 24 hours following a traumatic injury [42]. Additionally, the risk of postoperative complications in surgical patients is significantly influenced by the condition of wounded tissue. Surgeons encounter challenges such as iatrogenic harm, anastomotic leakages, and infections following abdominal surgeries or resections [43–46]. Given the direct impact on patient outcomes, addressing inadequate wound healing from a new perspective is of great interest. Several inventions have been employed successfully to integrate biological tissue. One of those technologies is tissue adhesive. These innovations can improve the effectiveness of clinical results by enhancing hemorrhage control. Elgazery and Elelamy [47] explored multiple solutions for non-Newtonian fluid over a stretching sheet with a nonlinear radiation case and analyzed the temperature in terms of transdermal drug delivery application. They successfully attained the performance of spreading the medication onto a flat sheet through the pertinent physical parameters. After getting motivated by these references, the present paper exhibits the novelty of considering the viscoinelastic nature of tissue adhesive, which influences the heat transfer estimation and examines the prospects of bioactive tissue adhesives onto a stretching sheet.

1.1. Contribution

The main focus of this paper is,

- To develop an incompressible two-dimensional Prandtl-Eyring nanofluid flow past a stretching surface loaded with the impact of Brownian motion and thermophoresis.

- To address the utilization of the NDSolve numerical method for simulating the behavior of the proposed model with the application of medicated tissue adhesive. This methodology reduces the complexity and provides an accurate solution in the least amount of CPU time.
- To forecast the nature of physical quantities across the entire region by employing a gradient descent approach. This algorithm is standardized by introducing a statistical indicator named mean squared error, which quantifies the exact difference between the actual value and predicted value.

Moreover, this work aims to enable a new perspective in fluid flow research in terms of prediction approach for the physical quantities, which can contribute to the development of new medical treatments and interventions. This approach offers an innovative idea for flow control and can potentially assist in simulating the governing boundary layer equations.

1.2. Structure

The structure of the paper is summarized below. The geometrical interpretation statement and mathematical description are provided in Section 2. The measurements of physical quantities are demonstrated in Section 3. The numerical and machine learning processes are explained in Sections 4 and 5, respectively. The graphical representations of computational solutions with physical attributes are illustrated in the final section. The concluding section covers the enumerated key points of the current analysis.

2. Flow Analysis

The steady, laminar, incompressible two-dimensional Prandtl-Eyring nanofluid flow over a stretched sheet is governed by the continuity and Navier–Stokes equations, as well as the Buongiorno design [48]. The velocity of the sheet in the x-direction is given by $U_w(x) = ax$. To control the flow direction, a transversely oriented magnetic field with potency B_0 is applied, as depicted in Figure 1. After addressing the boundary layer estimations, the system of equations for the Prandtl-Eyring nanofluid framework can be stated as follows [50]:

$$\frac{\partial u}{\partial x} + \frac{\partial v}{\partial y} = 0, \tag{2.1}$$

$$u\frac{\partial u}{\partial x} + v\frac{\partial u}{\partial y} = \frac{A}{\rho c}\frac{\partial^2 u}{\partial y^2} - \frac{A}{2\rho c^3}\left(\frac{\partial u}{\partial y}\right)^2\frac{\partial^2 u}{\partial y^2} - \frac{\sigma B_0^2}{\rho}u, \tag{2.2}$$

$$u\frac{\partial T}{\partial x} + v\frac{\partial T}{\partial y} = \frac{k}{\rho c_p}\left(\frac{\partial^2 T}{\partial y^2}\right) + \tau\left\{D_B\left(\frac{\partial C}{\partial y}\frac{\partial T}{\partial y}\right)\right\} + \tau\left\{D_T {T_\infty}^{-1}\left(\frac{\partial T}{\partial y}\right)^2\right\}, \tag{2.3}$$

$$u\frac{\partial C}{\partial x} + v\frac{\partial C}{\partial y} = D_B\left(\frac{\partial^2 C}{\partial y^2}\right) + D_T T_\infty^{-1}\left(\frac{\partial^2 T}{\partial y^2}\right), \tag{2.4}$$

in addition to the boundary constraints

$$\begin{cases} u = U_w(x),\ v = 0,\ T = T_w \text{ and } C = C_w \ at\ y = 0; \\ u \to 0,\ T \to T_\infty \text{ and } C \to C_\infty \ at\ y \to \infty. \end{cases} \tag{2.5}$$

In the aforementioned problem, u and v are the velocity components in the direction of x and y, respectively. The density, kinematic viscosity, and electrical conductivity of fluid are ρ, v, and σ. The fluid temperature is T, $\frac{k}{\rho c_p}$ is the heat diffusivity, C is the concentration of nanoparticles, D_B is the Brownian diffusion coefficient, D_T is the thermophoresis coefficient, and the ratio of the efficient thermal range of the nanoparticle material to the efficient thermal range of base fluid is τ. The material parameters are represented by A and c. The scaling group of conversions that transformed the governed partial differential equations (2.1-2.4) to ordinary differential equations are described below,

$$\begin{cases} \eta = \left(\frac{a}{v}\right)^{\frac{1}{2}} y, \quad \psi(x,y) = (av)^{\frac{1}{2}} x f(\eta), \\ \theta(\eta) = \frac{T - T_\infty}{T_w - T_\infty}, \quad \phi(\eta) = \frac{C - C_\infty}{C_w - C_\infty}. \end{cases} \tag{2.6}$$

Using Equation (2.6) in (2.1-2.4), gives

$$\alpha\Big[f''' - \beta f''^2 f'''\Big] + f f'' - f'^2 - M f' = 0, \tag{2.7}$$

$$\theta'' + Pr f\theta' + \frac{1}{Pr^{-1}}\Big[Nb\theta'\phi' + Nt\theta'^2\Big] = 0, \tag{2.8}$$

$$\phi'' + PrLef\phi' + NtNb^{-1}\theta'' = 0, \tag{2.9}$$

along with the boundary conditions

$$\begin{cases} f(\eta \to 0) = 0, \ f'(\eta \to 0) = 1, \ f'(\eta \to \infty) = 0; \\ \theta(\eta \to 0) = 1, \ \theta(\eta \to \infty) = 0; \\ \phi(\eta \to 0) = 1, \ \phi(\eta \to \infty) = 0. \end{cases} \tag{2.10}$$

In (2.7-2.9), α and β are designated to represent the Prandtl-Eyring parameters. The notation M stands for the Hartmann number, Nt, and Nb are symbolized to describe the thermophoresis and Brownian motion parameters, Le and Pr represent the Lewis number and Prandtl number, respectively. These expressions are followed by

$$\begin{cases} \alpha = \frac{A}{\mu c}, \ \beta = \frac{a^3 x^2}{2c^2 v}, \ M = \frac{\sigma B^2}{a\rho}, \ Nb = \frac{\tau D_B (C_w - C_\infty)}{v}, \\ Nt = \frac{\tau D_T (T_w - T_\infty)}{T_\infty v}, \ Pr = \frac{v\rho c_p}{k}, \ Le = \frac{k}{\rho c_p D_B}. \end{cases}$$

3. Physical Quantities

The mathematical expression of the wall drag coefficient, wall heat and mass fluxes are depicted as

$$C_{fx} = \frac{\tau_w}{\frac{1}{2}\rho U_w^2}, \ Nu_x = \frac{x q_w k^{-1}}{T_w - T_\infty}, \ Sh_x = \frac{x q_m {D_B}^{-1}}{C_w - C_\infty}. \tag{3.1}$$

The representation of wall shear stress τ_w, wall thermal gradient q_w, and wall mass gradient q_m are presented by,

$$\begin{cases} \tau_w = \dfrac{A}{c}\left(\dfrac{\partial u}{\partial y}\right)_{y=0} - \dfrac{A}{6c^3}\left(\dfrac{\partial u}{\partial y}\right)^3_{y=0}, \\ q_w = -k\left(\dfrac{\partial T}{\partial y}\right)_{y=0}, \quad q_m = -D_B\left(\dfrac{\partial C}{\partial y}\right)_{y=0}. \end{cases} \tag{3.2}$$

After comprising the dimensionless variables in equations (3.1, 3.2), shear rate coefficient, heat transfer coefficient and concentration flux number are accounted in the subsequent form:

$$\begin{cases} \dfrac{1}{2}C_{fx}Re_x^{\frac{1}{2}} = \alpha\Big\{f''(0) - \dfrac{\beta}{3}[f''(0)]^3\Big\}, \\ \dfrac{Nu_x}{Re_x^{\frac{1}{2}}} = -\theta'(0), \\ \dfrac{Sh_x}{Re_x^{\frac{1}{2}}} = -\phi'(0). \end{cases} \tag{3.3}$$

M	Fatehzadeh et al. [49]	Zahra et al. [50]	Akbar et al. [51]	Current findings
0	-1	-1.004	-1	-1.0014
0.5	-	-1.1180	-1.11803	-1.22491
1.0	-1.41412	-1.4140	-1.41421	-1.41424
5.0	-2.44948	-2.4494	-2.44949	-2.44949
10	-3.31662	-3.3168	-3.31663	-3.31662

Table 1. Comparison result of $f''(0)$ with respect to the Hartmann number M when α=1, β=0.

4. Solution Methodology

The ordinary differential equations (2.7-2.9) and the relevant boundary constraints (2.10) are scientifically evaluated for different values of the pertinent parameters operating a Wolfram Language program, such as Prandtl-Eyring fluid parameters, Hartmann number, Prandtl number, Lewis number, Brownian motion, and thermophoresis parameter. All graphs observe the default significances of $\alpha = 5.0, \beta = 0.4, M = 0.5, Pr = 0.7, Le = 3.0, Nb = 0.1,$ and $Nt = 0.1$, excluding accentuated on the graph. A 3D graph provides an exact description of a physical significance and shows how the scale of the response is represented.

5. Machine Learning Technique

An innovation of the existing investigation lies in the implementation of supervised learning algorithm, which deals with labeled datasets. Additionally, it aims to discover the regression function $\mathcal{Y}_{(pred)} = \mathcal{F}$ with input factors $\mathcal{X}$ as parameters and output factor $\mathcal{Y}_{(pred)}$ as physical quantities. The simple linear regression is a structural design of an iterative gradient descent algorithm. The best fitting line for skin friction coefficient, local Nusselt number, and local Sherwood number with respect to the wide range of

related parameters, are attained with the help of the Python Language. If b_0, m_0, $\mathcal{X}$, and $\mathcal{Y}_{pred}$ are the bias term, weight term, input, and predicted factor in a linear regression formation, then:

$$\mathcal{Y}_{(pred)} = m_0\mathcal{X} + b_0$$

The mean square error is computed when the predictive model is being trained, and it is a helpful metric for estimating the difference between the actual and forecasted values. The error values are getting decreased in each iteration. This iterative procedure continues to determine the line that exactly correlates with the given data points.

Parameter Values		**True Value** ($f''(0)$)	**Predicted Value**($f''(0)$)	Error
$\beta = 0.4$, $M = 0.5$, Pr=0.7, Le=3.0, $Nb = Nt$=0.1	α=4	-3.04376	-3.03048	3.5e-04
	α=5	-2.74673	-2.77327	
	α=6	-2.52934	-2.51606	
α=5.0, $M = 0.5$, Pr=0.7, Le=3.0, $Nb = Nt$=0.1	β=0.5	-2.77013	-2.76741	3.45e-05
	β=0.9	-2.88406	-2.89221	
	β=1.1	-2.96006	-2.95462	
α=5.0, $\beta = 0.4$, Pr=0.7, Le=3.0, $Nb = Nt$=0.1	M=0.5	-2.74673	-2.74831	1.64e-05
	M=1	-3.13329	-3.12772	
	M=1.2	-3.27552	-3.27949	

Table 2. True and predicted values of Skin friction coefficient($f''(0)$).

Parameter Values		**True Value** ($-\theta'(0)$)	**Predicted Value**($-\theta'(0)$)	Error
α=5.0, β=0.4, $M = 0.5$, Pr=0.7, Le=3.0, Nt=0.1	Nb=0.5	0.41518	0.41202	1.99e-05
	Nb=1.0	0.32111	0.32744	
	Nb=1.5	0.24602	0.24286	
α=5.0, $\beta = 0.4$, M=0.5, Pr=0.7, Le=3.0, Nb=0.1	Nt=0.1	0.50611	0.50412	5.58e-06
	Nt=0.5	0.45241	0.45573	
	Nt=1.1	0.38447	0.38314	
α=5.0, $\beta = 0.4$, $M = 0.5$, Le=3.0, $Nb = Nt$=0.1	Pr=0.7	0.50611	0.50896	1.14e-05
	Pr=0.9	0.57378	0.56902	
	Pr=1.2	0.65722	0.65912	

Table 3. True and predicted values of Nusselt number($-\theta'(0)$).

Parameter Values		**True Value** ($-\phi'(0)$)	**Predicted Value**($-\phi'(0)$)	Error
α=5.0, β=0.4, $M = 0.5$, Pr=0.7, Le=3.0, Nt=0.1	Nb=0.5	1.00413	1.00667	1.29e-05
	Nb=1.0	1.0254	1.02030	
	Nb=1.5	1.03139	1.03393	
α=5.0, $\beta = 0.4$, M=0.5, Pr=0.7, Le=3.0, Nb=0.1	Nt=0.1	0.82012	0.75039	6.8e-03
	Nt=0.5	0.15567	0.27188	
	Nt=1.1	-0.39939	-0.44587	
α=5.0, $\beta = 0.4$, $M = 0.5$, Pr=0.7, $Nb = Nt$=0.1	Le=2.0	0.57598	0.57830	1.07e-05
	Le=2.5	0.70500	0.70037	
	Le=3.0	0.82012	0.82243	

Table 4. True and predicted value of Sherwood number($-\phi'(0)$.

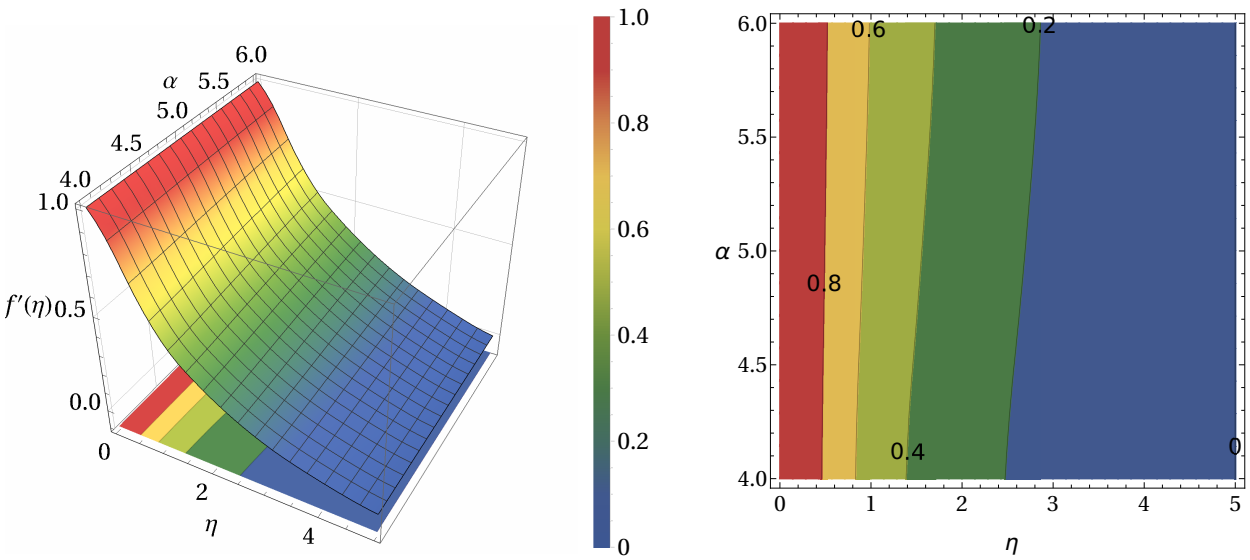

Figure 2. Influence of fluid parameter α on $f'(\eta)$.

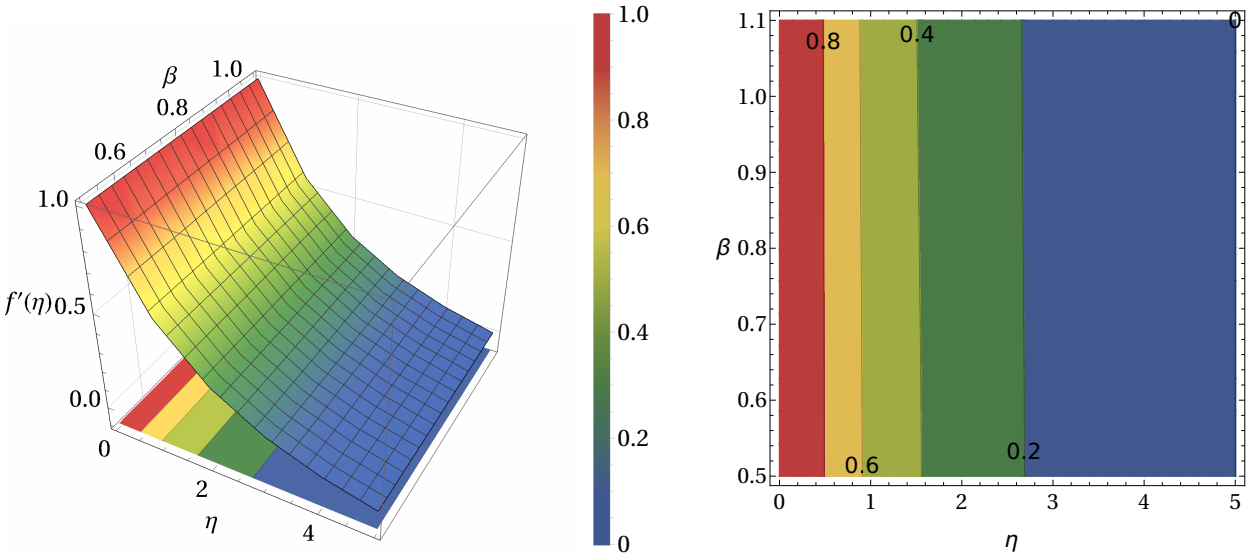

Figure 3. Influence of fluid parameter β on $f'(\eta)$.

6. Analysis and Discussion of Results

6.1. Velocity Profile

Figure 2 depicts the effect of the Prandtl-Eyring fluid parameter ($\alpha = 4, 5, 6$) on velocity distribution. In the boundary layer regime, the Prandtl-Eyring fluid parameter enhances momentum due to the reduction in viscous force for higher values of the parameter α. Consequently, for higher values of the material parameter α, the momentum layer significantly widens, as observed in the contour graph.

An impact of fluid parameter ($\beta = 0.5, 0.9, 1.1$) on velocity profile is adorned in Figure 3. The minor

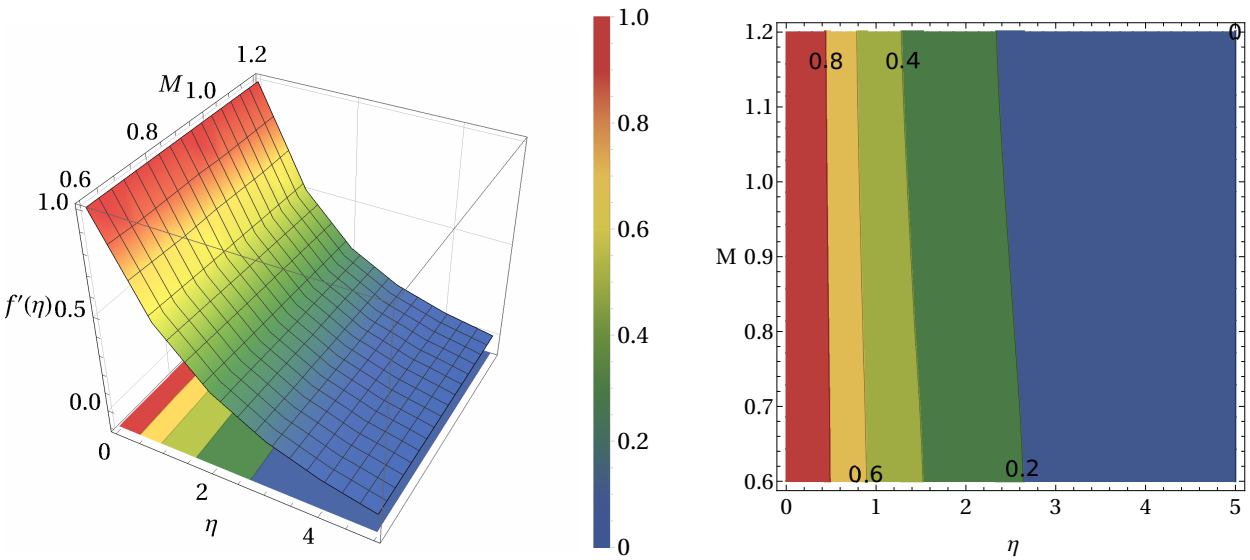

(a) (b)

Figure 4. Influence of Hartmann parameter M on $f'(\eta)$.

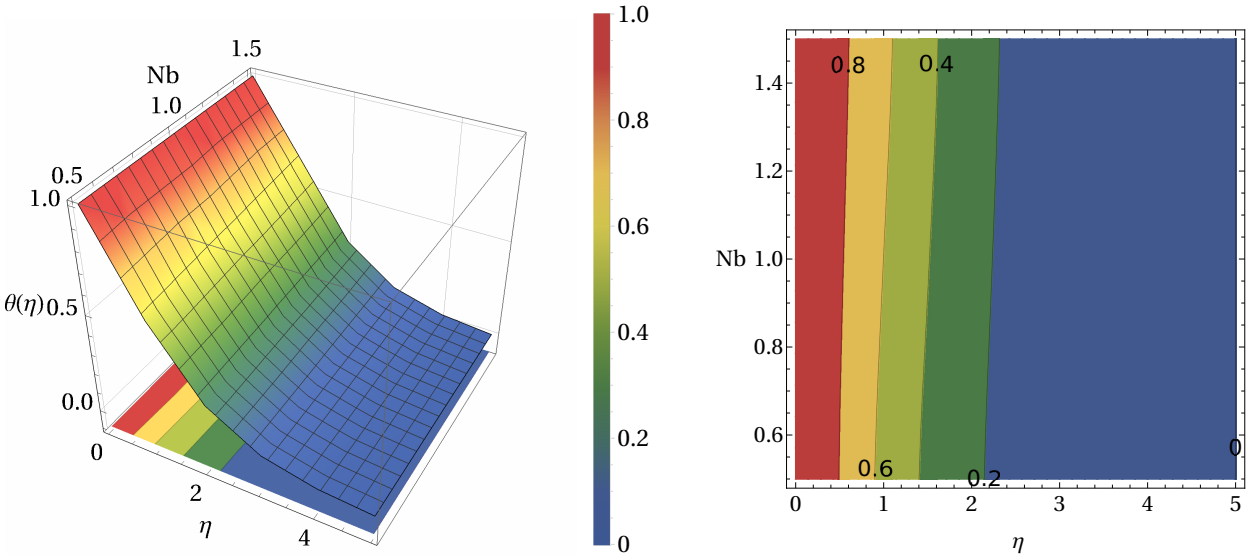

(a) (b)

Figure 5. Influence of Brownian motion parameter Nb on $\theta(\eta)$.

under-estimated fluid parameter values exhibit minimal linear momentum reduction in boundary layer thickness. The fact that the velocity curves overlap each other indicates that the fluid parameter β adjustment has negligibly changed the velocity field.

Figure 4 ensures the impact of Hartmann number ($M = 0.5, 1.0, 1.2$) on fluid velocity in the form of a contour graph. This figure demonstrates that the relation between independent variable η and velocity field display decimation. In further, amplifying the transverse magnetic field decreases the momentum profile. This crucial finding confirms that the magnetic field yields the Lorentz force, which diminishes the momentum. Therefore, a suitable magnetic field can be utilized to significantly handle blood flow during surgery.

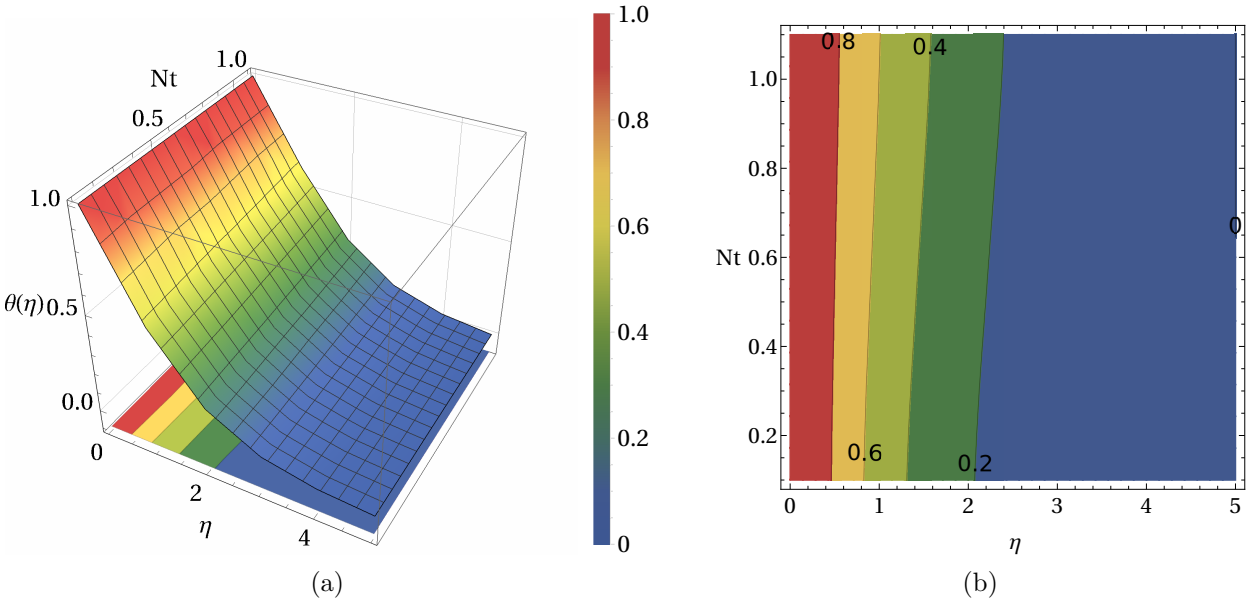

(a) (b)

Figure 6. Influence of thermophoresis parameter Nt on $\theta(\eta)$.

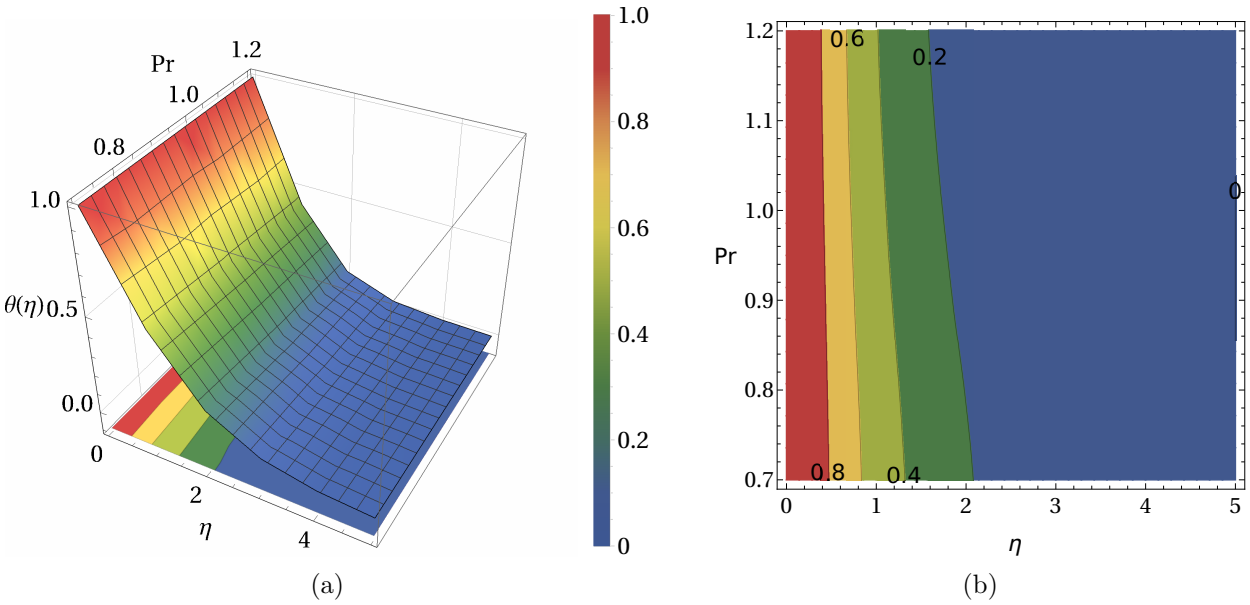

(a) (b)

Figure 7. Influence of Prandtl number Pr on $\theta(\eta)$.

A comparison of the obtained skin friction coefficient (i.e., $\alpha = 1$, $\beta = 0$) with the existing literature [49–51] is elucidated in Table 1. The impact of the Hartmann number ($M = 0, 0.5, 1.0, 5.0, 10.0$) on $f''(0)$ is validated by the precision of the proposed scientific scheme and determined to exhibit significant agreement. The current findings indicate its potential for hemorrhage control in biological tissue adhesion.

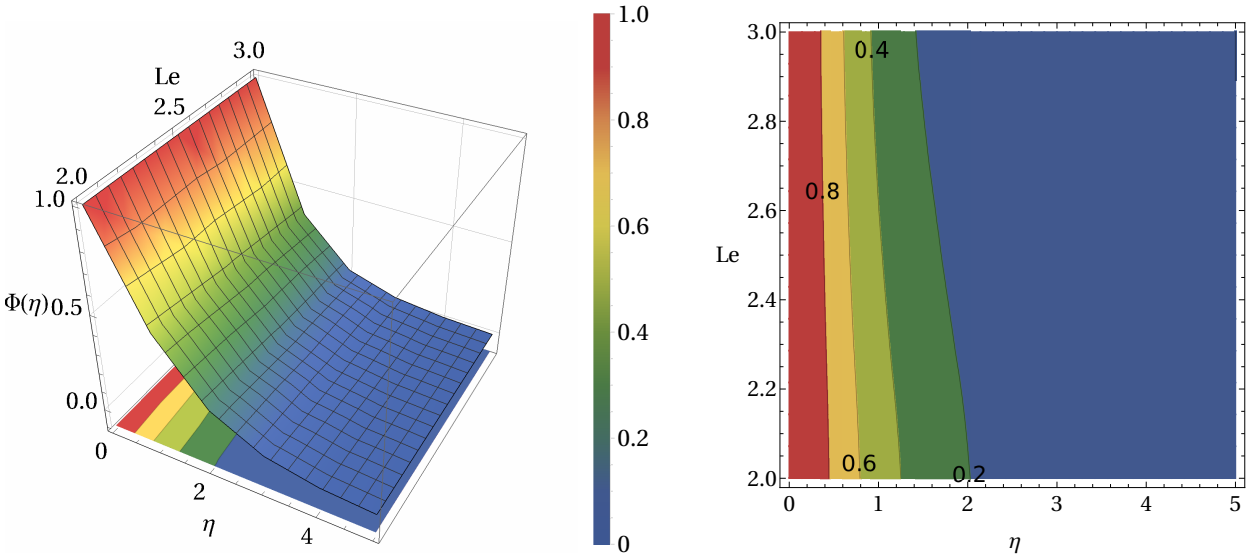

(a) (b)

Figure 8. Influence of Lewis number Le on $\phi(\eta)$.

6.2. Thermal and Concentration Profiles

The fluctuations of Brownian motion parameter ($Nb = 0.5, 1.0, 1.5$) on thermal field is elucidated in Figure 5. The random dispersion of nanoparticles in liquids is termed Brownian motion. The kinetic energy of the fluid molecules is converted into heat energy as a result of the random movement's intensification of the collision of nanoparticles with particles. As a result, the temperature rises. Furthermore, the thickness of the thermal boundary layer region is less than a strip of the boundary layer of momentum, as demonstrated in this graphical representation.

Figure 6 depicts the influence of the thermophoresis parameter ($Nt = 0.1, 0.5, 1.1$) on the temperature field. The present graph ensures the physical significance and shows a gradual rise in the thermal boundary layer for fewer variations of the thermophoresis parameter. Due to the fact that the thermophoresis mechanism leads particles to travel quickly from a heated continent to a cooler area. This consequence facilitates the transport of nanoparticles from a hot location to a cold one.

Figure 7 exhibits the consequence of Prandtl number ($Pr = 0.7, 0.9, 1.2$) on temperature profile. The value of the Prandtl number signifies the interaction between viscous and thermal conductivity. In physical phenomenon, the fluid with a higher value of the Prandtl number carries a downward thermal conductivity. This fact is attested to the current simulated outcomes, as seen in the Figure 7. The graphic illustrates that the higher Prandtl number leads the flow to drive contours towards the surface temperature that is extending or decreasing.

The contour effect of Lewis number ($Le = 2.0, 2.5, 3.0$) on the concentration distribution is enlightened in Figure 8. According to the description of the Lewis number, a more elevated Lewis number lessens the mass diffusivity. Physically, the diffusion coefficient diminishes due to the inverse relationship between Le and Nb. This figure proves that the concentration of nanoparticles and boundary layer thickness declines for an improving Lewis number.

Finally, Figure 9 illustrates the effect of the physical quantities on a broad range of pertinent parameters, such as α, β, M, Nb, Nt, Pr, and Le. In these regression graphs, the numerical and anticipated data points lie close to the diagonal line and are located along it. Furthermore, Table. 2-4 explores the true and forecasted results of the proposed model. Also, it provides the difference between true and predicted values in the name of mean squared error. The expected outcomes closely resemble the numerical

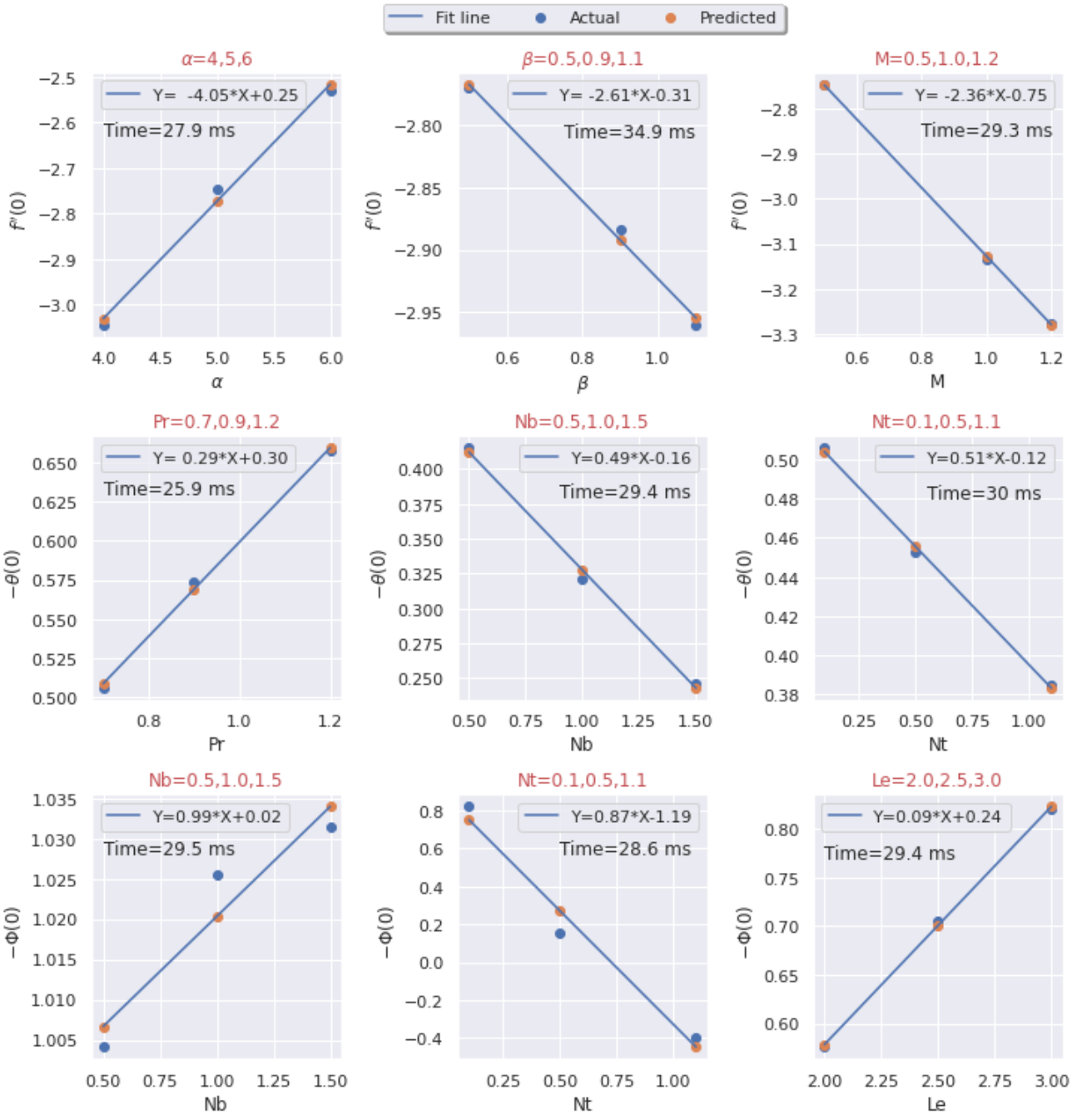

Figure 9. True Vs Predicted values of physical quantities.

values with minimal error. Accordingly, these patterns of technological advancement are expected to continue in the future, impacting computationally challenged sciences.

7. Enumerated Key points

The velocity, temperature, and concentration distributions of the Prandtl-Eyring nanofluid past a stretching surface phenomenon are numerically scrutinized. Moreover, machine learning is integrated based on the numerical findings to predict the physical quantities. The specific findings are as follows:

- The Prandtl-Eyring fluid parameter α upsurge the velocity profile. The features of thermophoresis and Brownian motion elevate the temperature.
- The Hartmann number M and Prandtl-Eyring fluid parameter β have an identical influence on fluid momentum, which improves the hemorrhage control in surgeries.
- The flow simulation is numerically treated by means of the NDSolve method and excellent agreement is found when compared to the Runge-Kutta-based shooting technique, homotopy perturbation method, and implicit finite difference method with quasi-linearization technique.
- The ML technique employed in this research executed well in forecasting the physical quantities of interest with minimal error 10^{-3}.
- An incorporation of numerical and machine learning techniques successfully observed the solution for the prospects of bioactive tissue adhesives onto a stretching sheet. It will be helpful for future endeavors in means of heat transfer estimation, which optimize the adhesion process and predict the delivery of medication to target areas.

The current findings reveal that it has a great potential for blood flow control in surgeries. Hence, the proposed numerical technique and regression analysis improve the application of the viscoinelastic flow regime in medicated tissue adhesive.

Nomenclature

$\alpha,\ \beta$	Non-dimensional fluid parameters
η	Space variable
$\mathcal{Y}$	True value
$\mathcal{Y}_{(pred)}$	Predicted value
μ	Dynamic viscosity($kgm^{-1}s^{-1}$)
ϕ	Dimensionless concentration
$\psi(x,y)$	Stream function
ρ	Density of the fluid(kgm^{-3})
σ	Electrical conductivity(sm^{-1})
τ	Effective heat capacity of the nanoparticle
τ_w	wall shear stress(Wm^{-2})
θ	Dimensionless temperature
A	Material parameter(kg/ms^2)
a	Stretching Parameter(1/s)
B_0	Magnetic Field($Tesla$)
b_0	Bias term
C	Concentration
c	Material parameter($1/s$)
c_p	Specific heat($Jkg^{-1}K^{-1}$)
C_∞	Free stream concentration
C_{fx}	Skin friction coefficient
D_B	Brownian diffusion coefficient(m^2/s)
D_T	Thermophoresis diffusion coefficient
f	Dimensionless velocity

$k/\rho c_p$	Thermal diffusivity($m^2 s^{-1}$)
Le	Lewis number
M	Hartmann parameter
m_0	Weight term
Nb	Brownian motion parameter
Nt	Thermophoresis parameter
Nu_x	Local Nusselt number
Pr	Prandtl number
q_m	Mass flux($kg/m^2 s$)
q_w	Heat flux(Wm^{-2})
Re_x	Local Reynolds number
Sh_x	Local Sherwood number
T	Temperature(K)
T_∞	Ambient temperature
u, v	Velocity components(ms^{-1})
$U_w(x)$	Stretching velocity(ms^{-1})
v	Kinematic viscosity($m^2 s^{-1}$)
x, y	Horizontal and vertical coordinates(M)

References

[1] B.C. Sakiadis, Boundary layer behavior on continuous solid flat surfaces, *AlChE Journal*, 1961, vol. 7, pp. 26–28.

[2] F.K. Tsou, E.M. Sparrow and R.J. Goldstein, Flow and heat transfer in the boundary layer on a continuous moving surface, *International Journal of Heat and Mass Transfer*, 1967, vol. 10, pp. 219–235.

[3] L. Crane, Flow past a stretching plate, *Zeitschrift für angewandte Mathematik und Physik ZAMP*, 1970, vol. 21, pp. 645–647.

[4] Zeeshan, I. Khan, N. Feroz, F. S. Al-Duais and O. Mahmoud, Visualization of non-Newtonian convective fluid flow with internal heat transfer across a rotating stretchable surface impact of chemical reaction, *Scientific Reports*, 12, 2022, 10392.

[5] A. S. M. Aljaloud, L. Manai and I. Tlili, Bioconvection flow of Cross nanofluid due to cylinder with activation energy and second order slip features, *Case Studies in Thermal Engineering*, 42, 2023, 102767.

[6] D. Pal, G. Mandal and K. Vajravalu, Soret and Dufour effects on MHD convective–radiative heat and mass transfer of nanofluids over a vertical non-linear stretching/shrinking sheet, *Applied Mathematics and Computation*, 2016, vol. 287-288, pp. 184-200.

[7] B.C. Prasannakumara, B.J. Gireesha, M.R. Krishnamurthy and K. Ganesh Kumar, MHD flow and nonlinear radiative heat transfer of Sisko nanofluid over a nonlinear stretching sheet, *Informatics in Medicine Unlocked*, 2017, vol. 9, pp. 123-132.

[8] F. Khani, A. Aziz and S. Hamedi-Nezhad, Simultaneous heat and mass transfer in natural convection about an isothermal vertical plate, *Journal of King Saud University - Science*, 2012, vol. 24, pp. 123-129.

[9] M. Irfan and M. Asif Farooq, Thermophoretic MHD free stream flow with variable internal heat generation/absorption and variable liquid characteristics in a permeable medium over a radiative exponentially stretching sheet, *Journal of Materials Research and Technology*, 2020, vol. 9, pp. 4855-4866.

[10] A. Felicita, B.J. Gireesha, B. Nagaraja and P. Venkatesh, Mixed convective flow of Casson nanofluid in the microchannel with the effect of couple stresses: irreversibility analysis, *International Journal of Modelling and Simulation*, 2023, 1-15.

[11] Yi-Xia Li, M. H. Alshbool, L. V. Yu-Pei, I. Khan, M. Riaz Khan and A. Issakhov, Heat and mass transfer in MHD Williamson nanofluid flow over an exponentially porous stretching surface, *Case Studies in Thermal Engineering*, 2021, vol. 26.

[12] R. Jusoh, R. Nazar and I. Pop, Flow and heat transfer of magnetohydrodynamic three-dimensional Maxwell nanofluid over a permeable stretching/shrinking surface with convective boundary conditions, *International*

Journal of Mechanical Sciences, 2017, vol. 124-125, pp. 166-173.
[13] J. Zhang and L. V. Yanhui, High-order finite element method on a Bakhvalov-type mesh for a singularly perturbed convection-diffusion problem with two parameters, *Applied Mathematics and Computation*, 2021, vol. 397, 125953.
[14] A. M. Rashad, A. J. Chamkha and M. Modather, Mixed convection boundary-layer flow past a horizontal circular cylinder embedded in a porous medium filled with a nanofluid under convective boundary condition, *Computers and Fluids*, 2013, vol. 86, pp. 380-388.
[15] A. Hussain and M.Y. Malik, MHD nanofluid flow over stretching cylinder with convective boundary conditions and Nield conditions in the presence of gyrotactic swimming microorganism: A biomathematical model, *International Communications in Heat and Mass Transfer*, 2021, vol. 126, 105425.
[16] Q. H. Le, Z. Hussain, N. Khan, S. Zuev, K. Javid, S. U. Khan, Z. Abdelmalek and I. Tlili, Chebyshev collocation simulations for instability of Hartmann flow due to porous medium: A neutral stability and growth rate assessment, *Ain Shams Engineering Journal*, 2023, 102215.
[17] O. D. Makinde and A. Aziz, Boundary layer flow of a nanofluid past a stretching sheet with a convective boundary condition, *International Journal of Thermal Sciences*, 2011, vol. 50, pp. 1326-1332.
[18] S. Nasir, S. Islam, T. Gul, Z. Shah, M. Altaf Khan, W. Khan, A. Zeb Khan and S. Khan, Three-dimensional rotating flow of MHD single wall carbon nanotubes over a stretching sheet in presence of thermal radiation, *Applied Nanoscience*, 2018, vol. 8, pp. 1361–1378.
[19] P. M. Patil and B. Goudar, Time-dependent mixed convection of Prandtl–Eyring hybrid nanofluid flow over a vertical cone: Entropy analysis, *Asia-Pacific Journal of Chemical Engineering*, 2023.
[20] S. Chaudhary and K.K. Chouhan, Darcy-Forchheimer flow of Prandtl-Eyring nanofluid subjected to a Riga plate of varying thickness along with Brownian diffusion, thermophoresis and non-uniform heat source/sink effects, *Numerical Heat Transfer, Part A: Applications*, 2022.
[21] V. Puneeth, M. Shoaib Anwar and M. Riaz Khan, Bioconvective Darcy–Frochherimer flow of the Ree–Eyring nanofluid through a stretching sheet with velocity and thermal slips, *Waves in Random and Complex Media*, 2022, 1-22.
[22] D. Habib, N. Salamat, S. Hussain, B. Ali and S. Abdal, Significance of Stephen blowing and Lorentz force on dynamics of Prandtl nanofluid via Keller box approach, *International Communications in Heat and Mass Transfer*, 2021, vol. 128, 105599.
[23] N. S. Akbar, MHD Eyring–Prandtl fluid flow with convective boundary conditions in small intestines, *International Journal of Biomathematics*, 2013.
[24] N. S. Akbar, S. Nadeem and C. Lee, Biomechanical analysis of Eyring Prandtl fluid model for blood flow in stenosed arteries, *International Journal of Nonlinear Sciences and Numerical Simulation*, 2013, vol. 14, pp. 345-353.
[25] S. R. Munjam, K. Gangadhar, R. Seshadri and M. Rajeswar, Novel technique MDDIM solutions of MHD flow and radiative Prandtl-Eyring fluid over a stretching sheet with convective heating, *International Journal of Ambient Energy*, 2021.
[26] A. Hussain, M. Y. Malik, M. Awais, T. Salahuddin and S. Bilal, Computational and physical aspects of MHD Prandtl-Eyringfluid flow analysis over a stretching sheet, *Neural Computing and Applications volume*, 2019, vol. 31, pp. 425-433.
[27] T. Hayat, N. Aslam, A. Alsaedi and M. Rafiq, Numerical study for MHD peristaltic transport of Sisko nanofluid in a curved channel, *International Journal of Heat and Mass Transfer*, 2017, vol. 109, pp. 1281-1288.
[28] I. Ullah, M. Alghamdi, W. F. Xia, S. I. Shah and H. Khan, Activation energy effect on the magnetized-nanofluid flow in a rotating system considering the exponential heat source, *International Communications in Heat and Mass Transfer*, 2021, vol. 128, 105578.
[29] S. Nasir, Z. Shah, S. Islam, E. Bonyah and T. Gul, Darcy Forchheimer nanofluid thin film flow of SWCNTs and heat transfer analysis over an unsteady stretching sheet, *AIP Advances*, 2019.
[30] N.A. Treiber, J. Heinermann and O. Kramer, Wind power prediction with machine learning, in: Computational Sustainability, *Springer*, 2016, pp. 13-29.
[31] A. M. Rushdi, S. Yoshida, K. Watanabe and Y. Ohya, Machine learning approaches for thermal updraft prediction in wind solar tower systems, *Renewable Energy*, 2021, vol. 177, pp. 1001-1013.
[32] M.A. Rushdi, A.A. Rushdi, T.N. Dief, A.M. Halawa, S. Yoshida and R. Schmehl, Power prediction of airborne wind energy systems using multivariate machine learning, *Energies*, 2020, vol. 13 (9), 2367.

[33] C. Voyant, G. Notton, S. Kalogirou, M. L. Nivet, C. Paoli, F. Motte and A. Fouilloy, Machine learning methods for solar radiation forecasting: a review, *Renewable Energy*, 2017. vol. 105, 569-582.
[34] N. Sharma, P. Sharma, D. Irwin and P. Shenoy, Predicting solar generation from weather forecasts using machine learning, in: 2011 IEEE International Conference on Smart Grid Communications (SmartGridComm), *IEEE*, 2011, pp. 528-533.
[35] S. Kalogirou, Artifcial Intelligence in Energy and Renewable Energy Systems, *Nova Publishers*, 2007.
[36] S. B. Kotsiantis, Supervised machine learning: a review of classification techniques, *Informatica*, 2007, vol. 31, pp. 249-268.
[37] T. Hastie, R. Tibshirani and J. Friedman, Unsupervised learning. In: The Elements of Statistical Learning: Data Mining, Inference, and Prediction, *Springer Science and Business Media*, 2009, pp. 485-585.
[38] M. P. Brenner, J. D. Eldredge and J. B. Freund, Perspective on machine learning for advancing fluid mechanics, *Physical Review Fluids*, 2019, vol. 4, Article number 100501.
[39] P. Priyadharshini, M. Vanitha Archana, N. Ameer Ahammad, C.S.K. Raju, Se-jin Yook and Nehad Ali Shah, Gradient descent machine learning regression for MHD flow: Metallurgy process, *International Communications in Heat and Mass Transfer*, 2022, vol. 138, 106307.
[40] P. Priyadharshini and M. Vanitha Archana, Augmentation of magnetohydrodynamic nanofluid flow through a permeable stretching sheet employing Machine learning algorithm, *Examples and Counterexamples*, 2023, vol. 3, 100093.
[41] P. Priyadharshini, M. Vanitha Archana, N. A. Shah and M. H. Alshehri, Ternary Hybrid Nanofluid Flow Emerging on a Symmetrically Stretching Sheet Optimization with Machine Learning Prediction Scheme, *Symmetry*, 2023, vol. 15, 1225.
[42] D. S. Kauvar, R. Lefering and C. E. Wade, Impact of hemorrhage on trauma outcome: an overview of epidemiology, clinical presentations, and therapeutic considerations, *The Journal of Trauma*, 2006, PMID: 16763478, S3–11.
[43] H. A. Powell, L. J. Tata, D. R. Baldwin, R. A. Stanley, A. Khak wani and R. B. Hubbard, Early mortality after surgical resection for lung cancer: an analysis of the English National Lung cancer audit, *Thorax*, 2013, vol. 9, pp. 826-834.
[44] F. Daams, M. Luyer and J. F. Lange, Colorectal anastomotic leakage: Aspects of prevention, detection and treatment, *World Journal of Gastroenterol*, 2013, vol. 15, pp. 2293-2297.
[45] T. Jakobson, J. Karjagin, L. Vipp, M. Padar, A. H. Parik, L. Starkopf, H. Kern, O. Tammik and J. Starkopf, Postoperative complications and mortality after major gastrointestinal surgery, *Medicina (Kaunas)*, 2014, vol.50(2), pp.111-117.
[46] M. T. Matter, F. H. L. Starsich, M. Galli, M. Hilber, A. A. Schlegel, S. Bertazzo, S. E. Pratsinis and I. K. Herrmann, Developing a tissue glue by engineering the adhesive and hemostatic properties of metal oxide nanoparticles, *Nanoscale*, 2017, vol. 9, pp. 8418-8426.
[47] N. S. Elgazery and A. F. Elelamy, Multiple solutions for non-Newtonian nanofluid flow over a stretching sheet with nonlinear thermal radiation: Application in transdermal drug delivery, *Pramana - J Phys*, 2020, vol. 94.
[48] J. Buongiorno, Convective Transport in Nanofluids, Journal of Heat Transfer, 2006, vol. 128(3).
[49] M. Fathizadeh, M. Madani, Y. Khan, N. Faraz, A. Yldrm and S. Tutkun, An effective modification of the homotopy perturbationmethod for MHD viscous flow over a stretching sheet, *Journal of King Saud University - Science*, 2019, vol. 25, pp. 107-113.
[50] A. Zahra, A. Hussain, S. Bilala, EI-Sayed M. Sherif and P. Thounthong, Brownian motion and thermophoretic diffusion influence on thermophysical aspects of electrically conduction nanofluid flow over a stretched surface, *Journal of Materials Research and Technology*, 2020, vol. 9, pp. 11948-11957.
[51] N. S. Akbar, A. Ebai and Z. H. Khan, Numerical analysis of magneticfield effects on Eyring-Powell fluid flow towards a stretching sheet, *Journal of Magnetism and Magnetic Materials*, 2015, vol. 382, pp. 355–358.